Preclinical targeting of the tumor microenvironment

Arjaans, Marlous

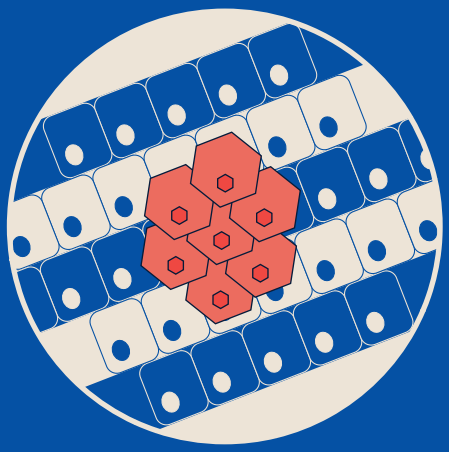

Chapter 5A

Bevacizumab-induced normalization of blood vessels in tumors hampers antibody uptake

Marlous Arjaans[1], Thijs H. Oude Munnink[1], Sjoukje F. Oosting[1], Anton G.T. Terwisscha van Scheltinga[1,3], Jourik A. Gietema[1], Erik T. Garbacik[4], Hetty Timmer-Bosscha[1], Marjolijn N. Lub-de Hooge[2,3], Carolina P. Schröder[1], and Elisabeth G.E. de Vries[1]

[1]Department of Medical Oncology, University Medical Center Groningen, Groningen, The Netherlands
[2]Department of Nuclear Medicine and Molecular Imaging, University of Groningen and University Medical Center Groningen, Groningen, The Netherlands
[3]Department of Hospital and Clinical Pharmacy, University of Groningen and University Medical Center Groningen, Groningen, The Netherlands
[4]Optical sciences group, MESA+ Institute for nanotechnology, University of Twente, Enschede, the Netherlands

Cancer Research 2013; 73: 3347-3355

Abstract

In solid tumors, angiogenesis occurs in the setting of a defective vasculature and impaired lymphatic drainage that is associated with increased vascular permeability and enhanced tumor permeability. These universal aspects of the tumor microenvironment can have a marked influence on intratumoral drug delivery that may often be underappreciated. In this study, we investigated the effect of blood vessel normalization in tumors by the antiangiogenic drug bevacizumab on antibody uptake by tumors. In mouse xenograft models of human ovarian and esophageal cancer (SKOV-3 and OE19), we evaluated antibody uptake in tumors by positron emission tomographic imaging 24 and 144 hours after injection of ^{89}Zr-trastuzumab (SKOV-3 and OE19), ^{89}Zr-bevacizumab (SKOV-3), or ^{89}Zr-IgG (SKOV-3) before or after treatment with bevacizumab. Intratumor distribution was assessed by fluorescence microscopy along with mean vessel density (MVD) and vessel normalization. Notably, bevacizumab treatment decreased tumor uptake and intratumoral accumulation compared with baseline in the tumor models relative to controls. Bevacizumab treatment also reduced MVD in tumors and increased vessel pericyte coverage. These findings are clinically important, suggesting caution in designing combinatorial trials with therapeutic antibodies due to a possible reduction in tumoral accumulation that may be caused by bevacizumab cotreatment.

Introduction

Angiogenesis, the formation of new blood vessels, is one of the hallmarks of cancer, and is therefore an anti-cancer drug target (1, 2). In solid tumors, extensive angiogenesis is accompanied by defective vascular architecture, leading to increased vascular permeability, hypoxia, low pH and high interstitial fluid pressure. Several preclinical and clinical studies indicate that anti-angiogenic drugs, including the anti-vascular endothelial growth factor-A (VEGF-A) antibody bevacizumab, lead to vessel normalization in addition to their antivascular effect. Major characteristics of vessel normalization include reduced number and size of immature vessels, increased vessel pericyte coverage, and reduced interstitial fluid pressure (3, 4). Normal (or normalized) blood vessels are lined with pericytes. This lining is absent in the abnormal, immature vessels created during tumor angiogenesis, which can cause increased leakiness (5).

In the process of vessel normalization, the architecture of the remaining vasculature is largely restored, leading to reduced vessel permeability and thereby improving tumor blood flow and tumor oxygenation (3-8). Bevacizumab is mainly given in combination with chemotherapy. One possible explanation for the beneficial effect of this combination therapy is subscribed to vessel normalization leading to increased tumor uptake of chemotherapy (7,9-13). However, in a recent clinical trial a single dose of 15 mg/kg bevacizumab reduced the tumor uptake of a radiolabeled docetaxel tracer dose from as early as 5 hours until 4 days after injection in non-small cell lung cancer patients (14). This finding does not necessarily indicate loss of efficacy of the combination, as had been shown in two bevacizumab and docetaxel containing neoadjuvant breast cancer trials (15,16).

The effects of vessel normalization may be even more important for the intratumoral delivery of macromolecular drugs, such as antibodies (17, 18). These effects might have implications for combination therapies, when bevacizumab is combined with other monoclonal antibodies. Although there is no clear evidence yet for this phenomenon at the tumor level, two large clinical colon cancer trials have shown that combining bevacizumab with cetuximab or panitumumab was less effective than either antibody alone (19, 20). Also, two randomized studies in patients with human epidermal growth factor receptor 2 (HER2) positive metastatic breast cancer showed disappointing impact of adding bevacizumab to trastuzumab (21, 22). It is therefore of interest to clarify whether bevacizumab impairs tumor uptake of other antibodies.

We have developed zirconium-89 (^{89}Zr) labeled bevacizumab and ^{89}Zr-trastuzumab as tracers for PET scanning to visualize and quantify bevacizumab and trastuzumab biodistribution for both preclinical and clinical purposes (23-25). These tracers can provide insight in how bevacizumab affects uptake of other antibodies.

We evaluated the effect of bevacizumab treatment on the tumor uptake of ^{89}Zr-trastuzumab, ^{89}Zr-bevacizumab and ^{89}Zr-Immunoglobulin G (IgG). In addition we tracked the localization of IgG in the tumors with *ex vivo* fluorescent labeling and related the findings to effects of bevacizumab treatment on tumor vessel density and vessel normalization.

Materials and methods

Antibody labeling

Trastuzumab (Roche), bevacizumab (Roche) and human IgG (Sanquin) were conjugated and labeled with ^{89}Zr as described previously (23, 25). IgG served as control, because it is biochemically comparable to trastuzumab and bevacizumab, but has no affinity for a specific antigen. In short, purified trastuzumab, bevacizumab and IgG were conjugated with the chelator tetrafluorphenol-N-succinyldesferal (TFP-N-sucDf) (kindly provided by Dr G.A. van Dongen, VUMC). Radiolabeling of all conjugates (N-sucDf-trastuzumab, -bevacizumab and -IgG) was performed with clinical grade ^{89}Zr-oxalate (IBA). All ^{89}Zr-tracers had a purity of >95% before administration to the animals.

IgG was also labeled with IRDye 800CW (LI-COR Biosciences) as described previously (26). Purified IgG was labeled with IRDye 800CW and the solution was purified with a PD-10 desalting column (GE Healthcare). Labeling efficiency and purity of IgG-800CW as determined by SE-HPLC were respectively 85-90% and >95%.

Animals and tumor inoculation

The human ovarian cancer SKOV-3 cell line was selected for xenograft experiments because of its high expression of VEGF and HER2 (25, 27). In addition, the HER2 overexpressing esophageal adenocarcinoma cell line OE19 (28) was used for xenograft experiments. Both tumor models had comparable tumor growth kinetics *in* vivo, which allowed the evaluation of both before- and during-treatment scans at a comparable tumor size. SKOV-3 was obtained from American Type Culture Collection (ATCC) and OE19 from Sigma Aldrich. Both cell lines were authenticated by STR profiling (Baseclear). ATCC HTB-77 was used as the reference profile for SKOV-3. The evaluation value (EV) obtained for SKOV-3 was 1 and for OE19 was 1.06. SKOV-3 cells were cultured in Dulbecco's modified Eagle medium (Invitrogen) and OE19 cells in Roswell Park Memorial Institute medium (Invitrogen), both with 4.5 g/mL glucose and supplemented with 10% fetal calf serum (FCS) at 37 °C in a humidified atmosphere containing 5% CO_2. For tumor inoculation the cells were harvested by trypsinization and resuspended in culture medium supplemented with FCS. *In vivo* imaging and *ex vivo* biodistribution experiments were conducted in male nude mice (HSD; Athymic nude-nu, average weight 30 g) obtained from Harlan.

In order to avoid a pharmacological effect of the ^{89}Zr-bevacizumab tracer, in the ^{89}Zr-bevacizumab group, a lower bevacizumab tracer dosage was essential to evaluate pre- and post-treatment tumor uptake. To enable imaging of low tracer dosages male nude mice (BALB/cOlaHDS-foxn^{nu}, average weight 20 g) from Harlan were used in the ^{89}Zr-bevacizumab group because of slower clearance of human IgG in these animals (29). At 6-8 weeks of age, mice were subcutaneously injected with 1x10^6 SKOV-3 cells or 3x10^5 OE19 cells in 0.3 mL Matrigel (BD Biosciences) and culture medium (1:1). Tumor growth was assessed by caliper measurements. When tumors measured 6-8 mm in diameter, ~2-3 weeks after inoculation, *in vivo* studies were started. All animal experiments were performed with isoflurane inhalation anesthesia (induction 3%, maintenance 1.5%). The animal experiments were approved by the Institutional Animal Care and Use Committee of the University of Groningen.

PET scan imaging and bevacizumab treatment

Clear tumor uptake of ^{89}Zr-trastuzumab and ^{89}Zr-bevacizumab is known to occur 24 hours post tracer injection with an optimal time point 144 hours after tracer injection (23, 25). Therefore, PET imaging was performed 24 or 144 hours after tracer injection. In the SKOV-3 model, on day 0 of the study schedule animals received the first tracer gift of ^{89}Zr-trastuzumab (100 µg, ± 5 MBq), ^{89}Zr-bevacizumab (10 µg, ± 5 MBq) or ^{89}Zr-IgG (100 µg, ± 5 MBq). In the OE19 model, animals received ^{89}Zr-trastuzumab (100 µg, ± 5 MBq) on day 0 of the study schedule. The tracers were injected intravenously (iv) in the penile vein. PET imaging was performed on day 1 and day 6 (respectively 24 and 144 hours post first tracer injection). From day 7 until 12 we allowed the tracer to decay and the antibody to remove form the tumor. On days 13, 16 and 19 the animals received a 5 mg/kg non-labeled treatment dose bevacizumab according to earlier studies or 0.9% NaCl as placebo (30). The second tracer injection was administered on day 14 and PET imaging was performed on day 15 and day 20 (respectively 24 and 144 hours post second radioactive tracer injection). Animals were sacrificed after the last scan on day 20. For the second tracer injection, both IgG groups received a co-injection of ^{89}Zr-(5 MBq) and IRDye 800CW-labeled IgG to study the intratumor distribution of IgG with fluorescence microscopy. The total protein dose was the same as in the first tracer injection, with half of the dose labeled fluorescently. In total five groups were scanned with different tracers and interventions: 1) ^{89}Zr-trastuzumab (n = 7), 2) ^{89}Zr-bevacizumab (n = 6), 3) ^{89}Zr-IgG (n = 6) all treated with bevacizumab, 4) ^{89}Zr-IgG (n = 6) treated with placebo all in the SKOV-3 model and 5) ^{89}Zr-trastuzumab (n = 6) in the OE19 model treated with bevacizumab. During each scan sequence static images of 15 minutes (24 hours post injection) and 45 minutes (144 hours post injection) acquisition time were obtained with a microPET

Focus 220 rodent scanner (CTI Siemens) followed by an 8-minute transmission scan. *In vivo* quantification was performed after image reconstruction with AMIDE Medical Image Data Examiner software (version 0.9.1). The data are presented as the mean standardized uptake value (SUVmean) and percentage injected dose per gram tissue (%ID/g).

***Ex vivo* biodistribution and tumor tissue analysis**

After the last PET scan on day 20, animals were sacrificed and organs were excised and weighted for biodistribution. Organs and primed standards were then counted for radioactivity in a calibrated well-type LKB-1282-Compu-gamma system (LKB Wallac) and corrected for physical decay. Hematoxylin and eosin (H&E) staining was performed to assess tumor viability for SKOV-3 and OE19. For immunohistochemistry and fluorescence imaging harvested tumors were formalin-fixed and paraffin-embedded. For SKOV-3 Slides (5 µm) were stained with antibodies against Ki67 (1:350, Dako) and von Willebrand Factor (vWF 1:250, Dako) to calculate the proliferation index and the mean vessel density (MVD) respectively. The proliferation index was calculated as the percentage of Ki67 positive nuclei in three fields at 400x magnification using a calibrated grid. The MVD was analyzed as described earlier (23). Angiogenic hot spot areas were determined in three predefined hot spot areas by counting the number of positive vessels at a 200x magnification using a calibrated grid. Images were acquired by the NanoZoomer 2.0-HT slide scanner (Hamamatsu). Tissue viability was expressed as the total percentage of necrosis in the tumor within fixed size squares overlaying the tumor sections. Analysis was performed using NanoZoomer Digital Pathology (NDP) viewer software (Hamamatsu). To visualize endothelial cells a fluorescent double staining with an antibody against Meca32 (1:40, BD Biosciences) was performed, while to visualize pericytes an antibody against α smooth muscle actin was used (SMA 1:100, Sigma). Nuclei were stained with Hoechst 33528 (1:5000, Molecular Probes, Invitrogen). Tumor sections were analyzed using a Leica DM6000 microscope and images shown were captured with a Leica DFC360FX camera and processed with LAS-AF2 software (Leica). In three predefined angiogenic hot spot areas, the degree of pericyte coverage was examined at a 200x magnification, and scored for no coverage, partial coverage, or full coverage.

Fluorescence microscopy analysis of IgG-800CW together with Hoechst staining was determined in tumor sections as described before (26) and overview images were obtained with the Odyssey infrared imaging system (LI-COR Biosciences). Image analysis was performed using FV10-ASW (version 1.6).

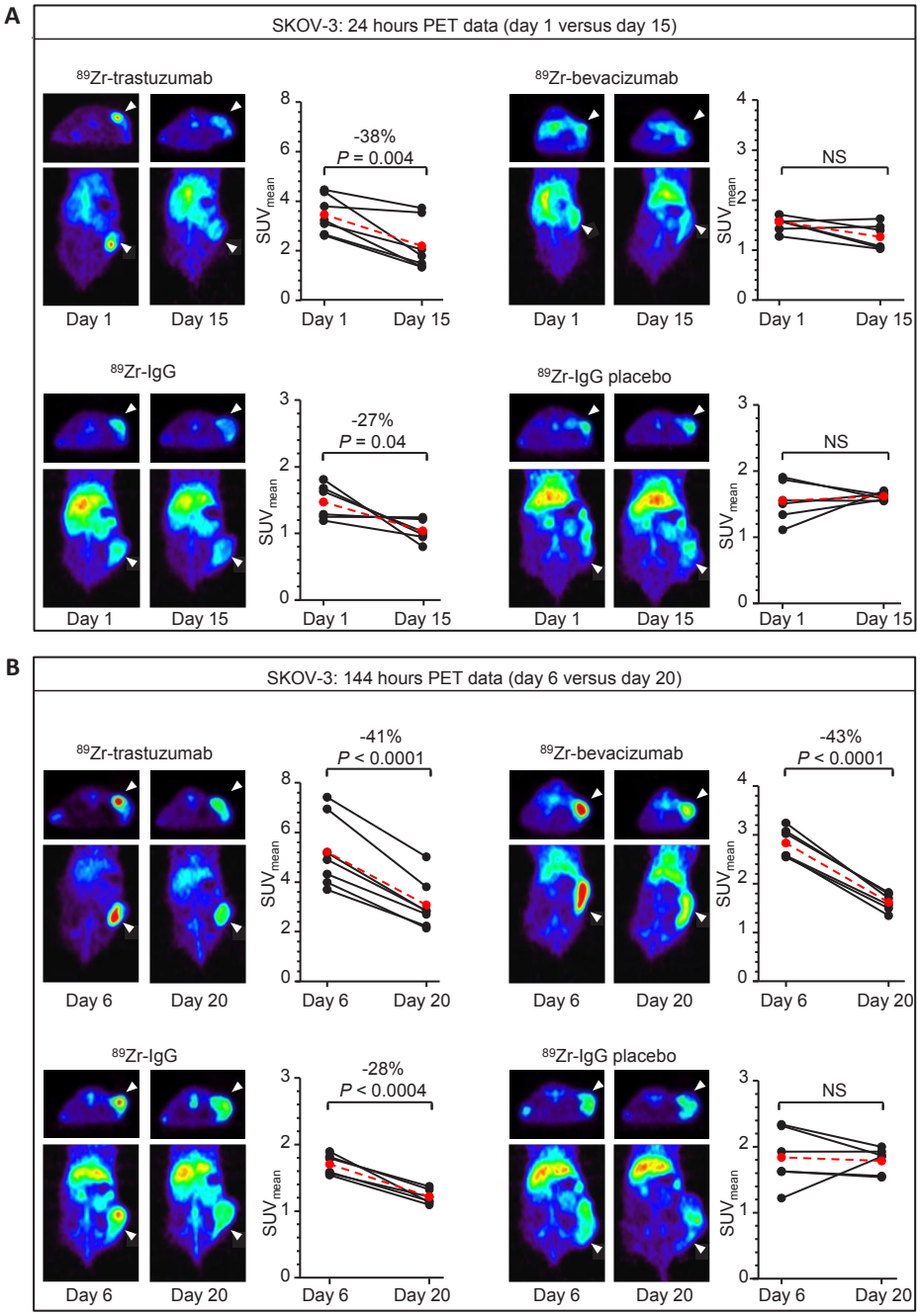

Fig. 1

SKOV-3 representative transversal and coronal microPET images of ^{89}Zr-trastuzumab, ^{89}Zr-bevacizumab and ^{89}Zr-IgG tumor uptake at (A) 24 hours (day 1 versus 15) and (B) at 144 hours (Day 6 versus 20) after tracer injection. Bevacizumab (5 mg/kg) or placebo treatment was given on day 13, 16 and 19. In the graphs, quantification of ^{89}Zr-trastuzumab, ^{89}Zr-bevacizumab and ^{89}Zr-IgG tumor uptake is shown for every individual animal (black) and the mean tumor uptake (dashed red line) expressed in SUV_{mean} ± SD. When the difference in tumor uptake before and after bevacizumab treatment was significant, the decrease (%) is given with corresponding *P* value.

Statistical Analysis

Data are presented as mean ± standard deviation (SD). PET data were analyzed with the paired Student's t-test. *Ex vivo* analysis was executed with the unpaired t-test. All statistical analyses were performed with Prism 5 (GraphPad). A *P* value of 0.05 or less (two-tailed) was considered significant.

Results

Bevacizumab treatment decreases tumor uptake of ^{89}Zr-trastuzumab, ^{89}Zr-bevacizumab and ^{89}Zr-IgG

PET images obtained at 24 and 144 hours after tracer injection visibly showed a lower tumor uptake of ^{89}Zr-trastuzumab, ^{89}Zr-bevacizumab and ^{89}Zr-IgG during bevacizumab treatment. Already on the 24 hours PET images after tracer injection (day 1 versus day 15), SUV_{mean} tumor uptake values decreased from 3.5 ± 0.8 to 2.2 ± 1.0 (-38 ± 20 %, *P* = 0.004), 1.5 ± 0.1 to 1.3 ± 0.3 (-16 ± 16 %, NS) and 1.5 ± 0.3 to 1.0 ± 0.2 (-27 ± 21 %, *P* = 0.04) for respectively ^{89}Zr-trastuzumab, ^{89}Zr-bevacizumab, and ^{89}Zr-IgG (Fig. 1A). This effect was even more pronounced at 144 hours (day 6 versus day 20), with a reduction in ^{89}Zr-trastuzumab tumor uptake from a SUV_{mean} of 5.2 ± 1.2 before to 3.0 ± 1.0 after bevacizumab treatment (-41 ± 5%, *P* < 0.0001) and a similar reduction in ^{89}Zr-bevacizumab tumor uptake with an SUV_{mean} of 2.8 ± 0.3 to 1.6 ± 0.2 after bevacizumab treatment (-43 ± 4%, *P* < 0.0001) (Fig. 1B).

Tumor uptake of ^{89}Zr-IgG was also lowered, although to a lesser extent. SUV_{mean} decreased from 1.7 ± 0.2 before to 1.2 ± 0.1 after bevacizumab treatment (-28 ± 6%, *P* = 0.0004).

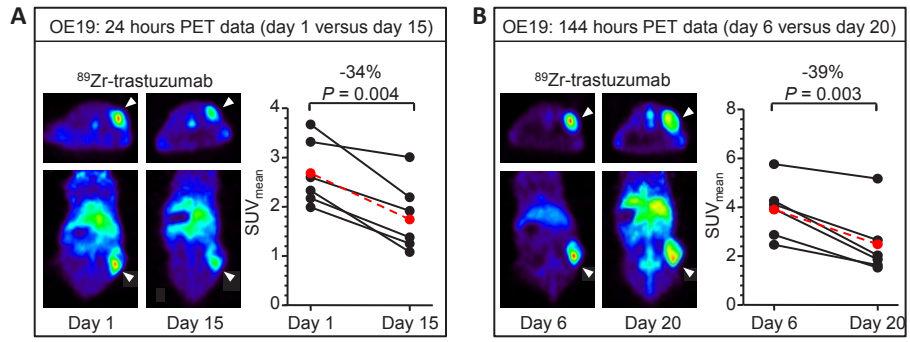

Fig. 2

OE19 representative transversal and coronal microPET images of ^{89}Zr-trastuzumab tumor uptake at (A) 24 hours (day 1 versus 15) and (B) 144 hours (day 6 versus day 20) after tracer injection. Bevacizumab (5 mg/kg) was given on day 13, 16 and 19. In the graphs, quantification of ^{89}Zr-trastuzumab tumor uptake is shown for every individual animal (black) and the mean tumor uptake (dashed red line) expressed in SUV_{mean} ± SD. When the difference in tumor uptake before and after bevacizumab treatment was significant, the decrease (%) is given with corresponding *P* value.

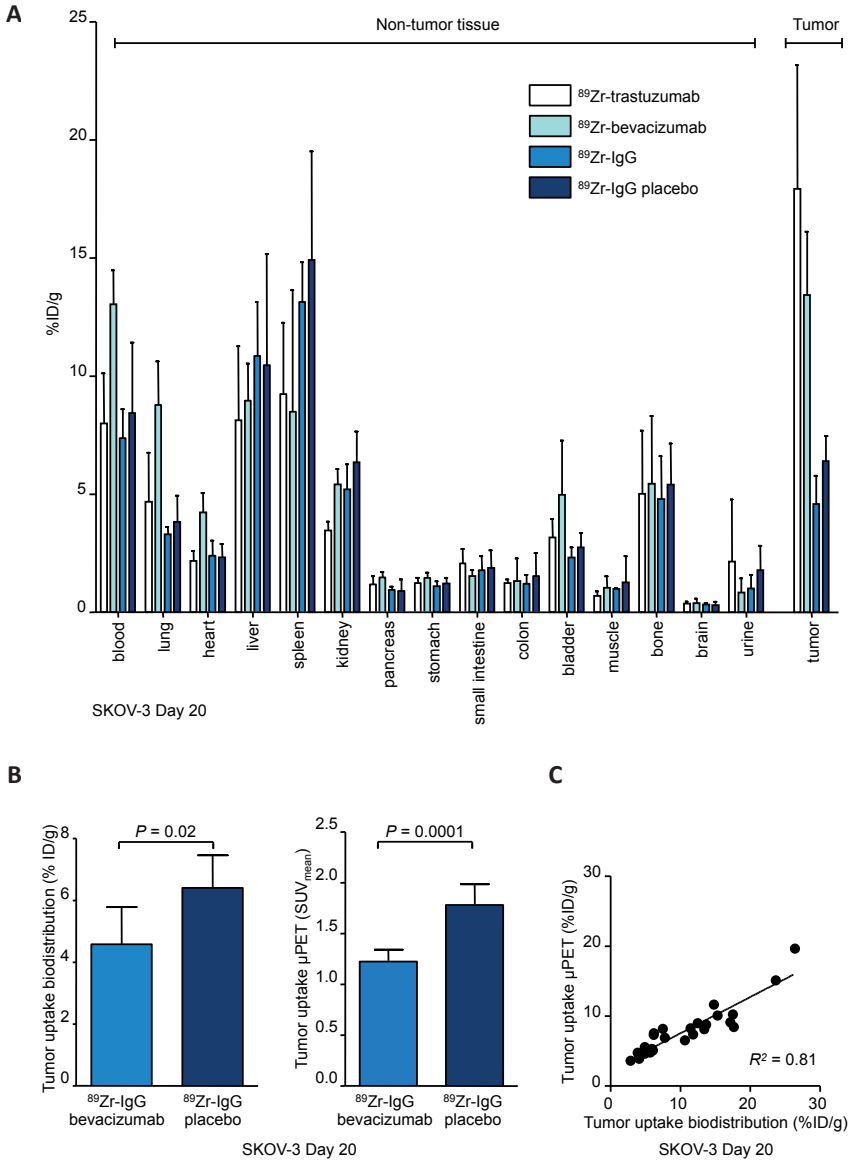

Fig. 3

(A) Day 20 *ex vivo* biodistribution data of the target specific tracers ^{89}Zr-trastuzumab, ^{89}Zr-bevacizumab and the aspecific tracer ^{89}Zr-IgG in mice bearing SKOV-3 treated with bevacizumab (5 mg/kg) or placebo on day 13, 16 and 19. The %ID/g ± SD is shown for non-tumor tissue and tumor for ^{89}Zr-trastuzumab, ^{89}Zr-bevacizumab and both ^{89}Zr-IgG groups. (B) Day 20 *ex vivo* biodistribution (%ID/g ± SD) and *in vivo* PET (SUV_{mean} ± SD) data of tumor uptake for the ^{89}Zr-IgG groups, treated with bevacizumab or placebo in the SKOV-3 model. Tumor uptake was lower in the ^{89}Zr-IgG group treated with bevacizumab, compared to the placebo treated ^{89}Zr-IgG group for biodistribution and PET data. (C) The day 20 *ex vivo* biodistribution tumor uptake (%ID/g) in the SKOV-3 model nicely correlated with the day 20 *in vivo* PET tumor uptake (%ID/g), R^2 = 0.81 for SKOV-3.

Placebo treatment did not affect ^{89}Zr-IgG uptake in the tumor with SUV_{mean} tumor uptake of 1.6 ± 0.3 before and 1.6 ± 0.1 after placebo at 24 hours and 1.8 ± 0.4 before and 1.8 ± 0.2 after placebo at 144 hours PET images (Fig. 1).

In the OE19 model, bevacizumab treatment also decreased the tumor uptake of ^{89}Zr-trastuzumab. Already on the 24 hours PET images (day 1 versus day 15), the SUV_{mean} tumor uptake values decreased from 2.7 ± 0.7 to 1.8 ± 0.7 (-34 ± 15 %, P = 0.004). At 144 hours (day 6 versus day 20), the SUV_{mean} tumor uptake decreased even more from 3.9 ± 1.2 to 2.5 ± 1.4 (-39 ± 16 %, (P = 0.003) (Fig. 2).

Ex vivo biodistribution of the tracer in non-tumor tissues and the tumor, for all four groups in the SKOV-3 model, are shown in Fig. 3A. *Ex vivo* biodistribution for both ^{89}Zr-trastuzumab and ^{89}Zr-bevacizumab were comparable to earlier described data, with high uptake of the tracer in the tumor, moderate uptake in the blood pool and highly vascularized organs and low uptake in the remaining organs. (23, 31). The *ex vivo* biodistribution data of ^{89}Zr-trastuzumab in the OE19 model was similar to the pattern in the SKOV-3 model (Supplemental Fig. 1A) For ^{89}Zr-IgG, tumor uptake was lower when the animals had received bevacizumab compared to the placebo treated ^{89}Zr-IgG group for both the *ex vivo* biodistribution tumor uptake (P = 0.02) and the *in vivo* PET tumor uptake (P = 0.0001) (Fig. 3B). Tumor uptake of the *in* vivo PET data nicely correlated with *ex vivo* tumor uptake as measured during biodistribution analysis for both the SKOV-3 (R^2 = 0.81, Fig. 3C) and the OE19 model (R^2 = 0.71) (Supplemental Fig. 1B).

Tumor growth and tumor size were comparable between all groups throughout the experiment, with no significant differences. For the SKOV-3 model, the average tumor size of all four tracer groups was 288 ± 66 mm^3 on day 1 and 494 ± 123 mm^3 on day 15. On day 6 this was 327 ± 74 mm^3 and 543 ± 86 mm^3 on day 20. For the OE19 model, on day 1 the average tumor size was 238 ± 71 mm^3 and 334 ± 117 mm^3 on day 15. On day 6 this was 298 ± 114 mm^3 and 404 ± 158 mm^3 on day 20.

Bevacizumab treatment normalizes the tumor vasculature and reduces uptake of fluorescent labeled IgG

Bevacizumab treatment reduced the tumor vessel density. In the placebo treated group the MVD was 9.0 ± 1.3 vessels/high power field, while the MVD in bevacizumab treated tumors was 5.8 ± 1.2 (P < 0.0003), 5.9 ± 1.1 (P = 0.0001) and 5.4 ± 0.8 (P < 0.0001) for the ^{89}Zr-trastuzumab, ^{89}Zr-bevacizumab and ^{89}Zr-IgG group respectively (Fig. 4A, C). Bevacizumab treatment also induced vessel normalization. In placebo treated tumors 68 ± 21% of the tumor vessels had no pericyte coverage and only 7 ± 11% of the vessels were fully covered with pericytes. After bevacizumab treatment pericyte coverage was absent in only 10 ± 14% of the tumor vessels (P < 0.0001), whereas 75 ± 21% of the

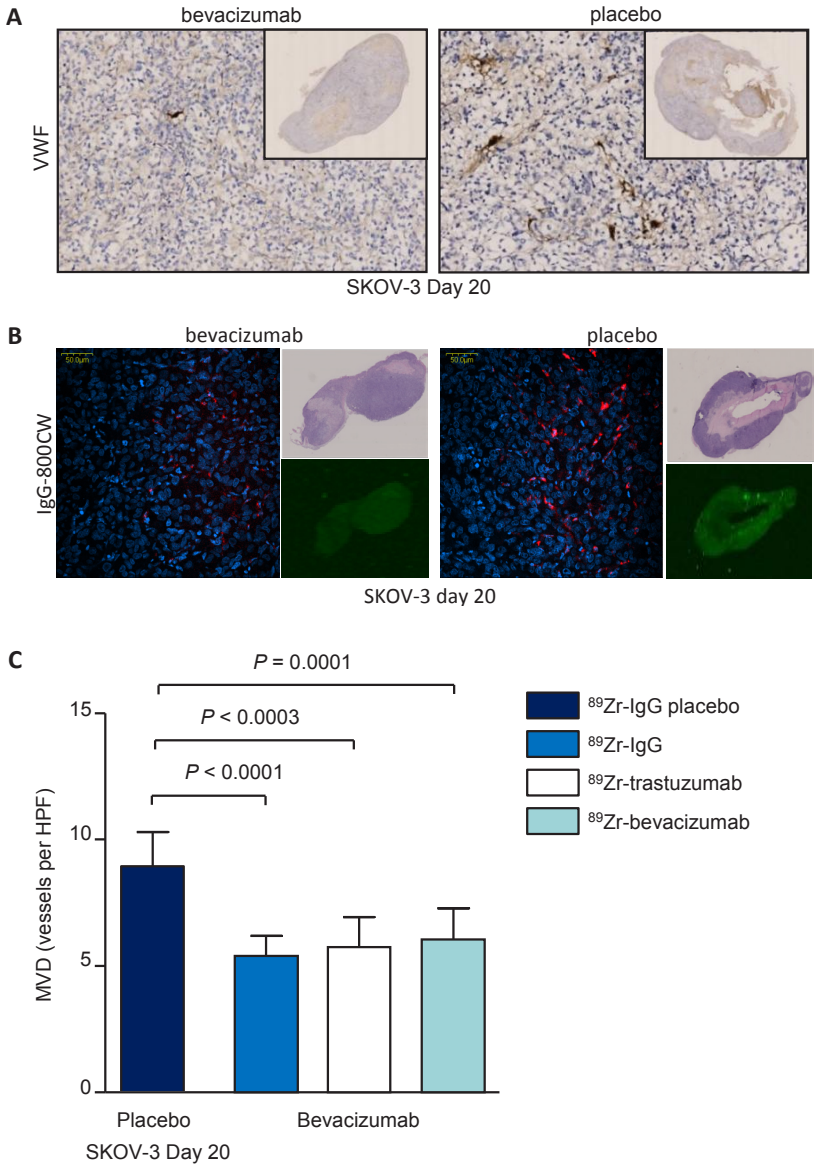

Fig. 4
(A) SKOV-3 day 20 representative images of depleted tumor vasculature in bevacizumab-treated tumors compared to placebo at 100x magnification. Insets depict overview images of the whole tumor. (B) SKOV-3 day 20 representative fluorescent images of IgG-800CW distribution throughout the tumor, illustrating less accumulation of IgG-800CW in bevacizumab-treated tumors compared to placebo (red: IgG-800CW, blue: Hoechst nuclei staining). Insets depict HE and fluorescent overview images of the whole tumor, showing increased uptake of IgG-800CW in areas of viable tumor tissue and necrosis. (C) SKOV-3 day 20 MVD depicted as vessels per high power field ± SD for ^{89}Zr-trastuzumab, ^{89}Zr-bevacizumab and both ^{89}Zr-IgG groups. Bevacizumab treatment (5 mg/kg on day 13, 16 and 19) decreased the MVD in all treatment groups, compared to placebo.

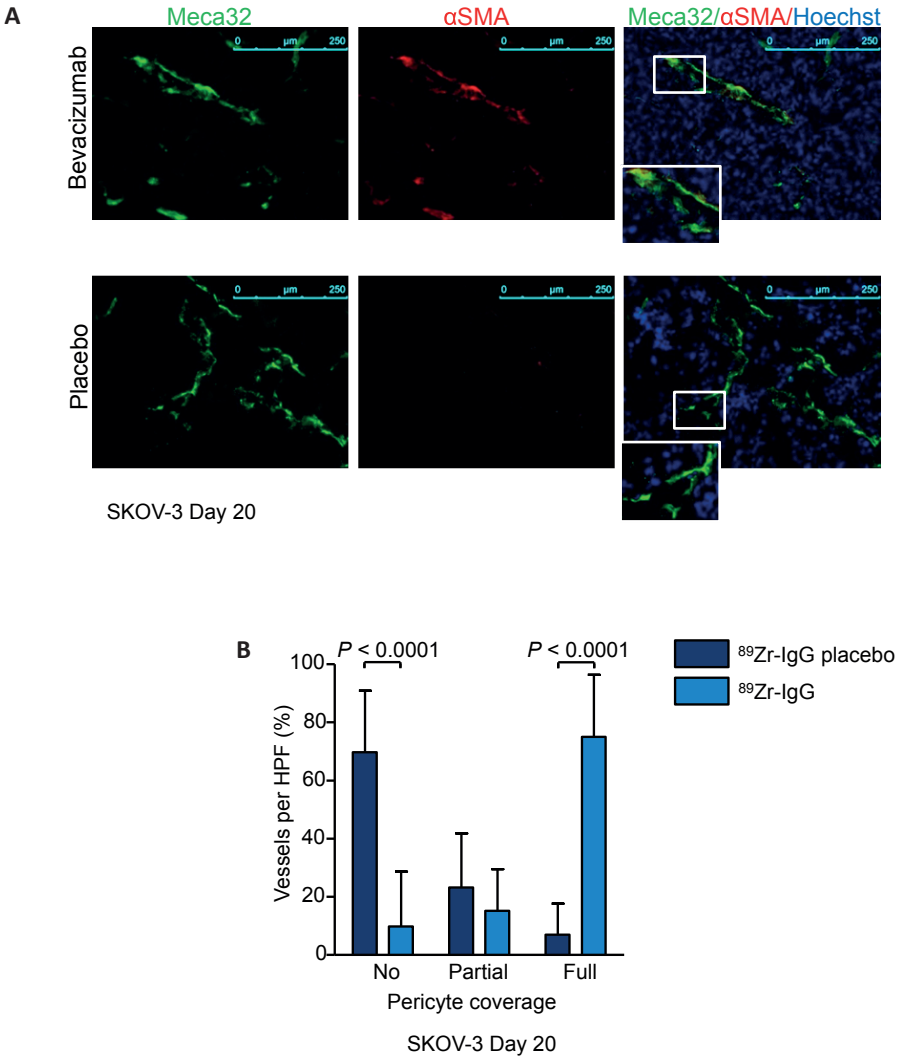

Fig. 5
(A) SKOV-3 day 20, representative examples of tumor tissue, showing tumor vasculature with and without pericyte coverage. From left to right: Meca32 staining, for the detection of endothelial cells and visualization of the tumor vasculature; αSMA staining for the detection of pericytes; and an overlay of Hoechst nuclei staining with Meca32 and αSMa. Bevacizumab-treated tumors showed tumor vasculature with substantial pericyte coverage compared to placebo. (B) SKOV-3 bevacizumab-treated tumors (5 mg/kg on day 3, 16 and 19) have more vessel pericyte coverage, compared to placebo treated tumors on day 20. Vessel pericyte coverage is defined as no, partial of fully covered expressed in vessels per high power field ± SD. Bevacizumab treatment induces a shift from tumor vessels with hardly any pericyte coverage to vessels mainly fully covered with pericytes.

vessels were fully covered ($P < 0.0001$) (Fig. 5). *Ex vivo*, we observed that IgG-800CW was mainly present in the extracellular matrix, and bevacizumab treatment reduced the accumulation of IgG-800CW relative to the placebo (Fig. 4B). This matches the PET results. Bevacizumab treatment did not affect tumor morphology and viability in both the SKOV-3 and OE19 model. In addition, bevacizumab did not affect the proliferation index in the SKOV-3 model.

Discussion

This study shows that bevacizumab treatment substantially reduces the tumor uptake of the antibodies trastuzumab, bevacizumab and of IgG. In addition, we show an induction of vessel normalization and decrease in MVD in these tumors by bevacizumab treatment. Since bevacizumab also lowered the uptake of IgG in the tumor, the results for the antibodies cannot solely be explained by a therapeutic effect or tumor saturation by bevacizumab itself. Therefore, these results demonstrate that bevacizumab treatment can impair penetration of large molecules such as antibodies into the tumor, resulting in a reduced tumor uptake of these antibodies.

In several preclinical settings such as murine mammary carcinoma, human small cell lung carcinoma, human glioblastoma multiforme, and human colon adenocarcinoma, blocking VEGF signaling not only led to a depletion of the vasculature, but also created a morphologically and functionally normalized vascular network of the remaining vessels (3, 4, 8, 32, and 33). There are also additional preclinical data supporting the effect of vessel normalization on drug uptake by tumors. In an orthotopic mammary model the effect of vessel normalization by antiangiogenic treatment was shown for uptake of nanomedicines ranging from 12 to 125 nm in size. The mice received 5 mg/kg of the mouse anti-VEGF antibody DC101 every 3 days. Intravital imaging showed that DC101 treatment led to vessel normalization in the tumor and thereby influenced the penetration of nanomedicines in the tumor. Small 12-nm particles took advantage of the induced vessel normalization, leading to better penetration of these particles into the tumor. Conversely, tumor uptake of 125-nm particles was reduced (34). We observed a reduction in tumor antibody uptake within 24 hours of tracer injection. This reduction was even more pronounced after 6 days, which coincided with a normalized tumor vasculature illustrated by increased pericyte coverage of the remaining vessels in the tumor.

Another recent study described the effect of a single administration of the species cross-reactive anti-VEGF-A antibody B20-4.1 24 hours prior to tracer injection on the biodistribution and pharmacokinetics of trastuzumab (35). Tumor bearing mice received trastuzumab labeled with the SPECT tracers Indium-111 (^{111}In) or Iodine-125 (^{125}I) and

were treated with or without B20-4.1. Biodistribution data showed a 25-30% decrease for both ^{111}In- and ^{125}I-trastuzumab tumor uptake for up to 7 days. SPECT-CT images made 2 days after anti-VEGF therapy also showed a decrease of ^{111}In-trastuzumab uptake in the tumor. The advantage of PET scanning which we used, over SPECT scanning is that it is easier to quantify uptake. We observed a 41% decrease *in vivo* of the PET tracer ^{89}Zr-trastuzumab tumor uptake after bevacizumab treatment. This decrease already occurred within one day after tracer injection and the start of bevacizumab treatment. Moreover we observed a decrease in uptake of ^{89}Zr-bevacizumab and ^{89}Zr-IgG after bevacizumab treatment.

We observed no effect on tumor size of bevacizumab treatment and ^{89}Zr-trastuzumab compared to placebo and ^{89}Zr-IgG, in the SKOV-3 model. This might be due to the fact that we treated the animals over a relatively short period of time (one week) with bevacizumab (5 mg/kg) and one single gift of trastuzumab (100 µg, corresponding with a dose of 4 mg/kg). However, there are only very limited preclinical data on the biological effect of combining bevacizumab with trastuzumab (36, 37). This will likely be due to the fact that testing antitumor efficacy of humanized antibodies in an animal model has its limitation since trastuzumab has inherent immunomodulatory activity (38-41). More importantly findings in the clinic show that bevacizumab treatment does not contribute favorably to the effect of trastuzumab and support the idea that vessel normalization by bevacizumab has the same effects in patients. In HER2 positive metastatic breast cancer patients, the combination of bevacizumab and trastuzumab showed only a minimal to no improvement in progression-free survival (21, 22). Combination studies of bevacizumab plus another antibody have shown a detrimental or only modestly beneficial effect. In colorectal cancer, bevacizumab and the epidermal growth factor receptor 1 (EGFR1) antibody cetuximab are both active drugs when combined with chemotherapy. In addition cetuximab has some activity as monotherapy (42, 43). But the combination of chemotherapy, bevacizumab and cetuximab even negatively affected the progression-free survival of colorectal cancer patients compared to chemotherapy and bevacizumab alone in the CAIRO 2 trial (19). A possible explanation of this reduced therapeutic efficacy was considered to be the fact that tumor-promoting M2 macrophages are activated by cetuximab in the local tumor microenvironment. This would lead to increased local VEGF production (44) resulting in insufficient depletion by bevacizumab. In addition, based on the present study, one could argue that the cetuximab levels in the tumors of these patients were likely lower because of the simultaneous treatment with bevacizumab. Analogously, in the PACCE trial, the addition of the EGFR1 antibody panitumumab to bevacizumab and chemotherapy in colorectal cancer patients also led to a decrease in progression-free survival (20). That vessel normalization by bevacizumab affects antibody

uptake in the clinic is supported by a preliminary report in which we showed a 47% lower tumor uptake of ^{89}Zr-bevacizumab after bevacizumab treatment in 11 renal cell cancer patients (45). Overall these clinical data are in line with a considerable biological effect of reduced antibody uptake after bevacizumab treatment.

PET scanning with ^{89}Zr-labeled antibodies can be used in future clinical studies as a supportive tool for more rationally designed treatment regimens containing bevacizumab combined with other antibodies. This can give additional insight whether choosing a treatment schedule affects tumor antibody distribution in patients and in this way PET imaging may contribute to improved and rational use of bevacizumab.

Disclosure of Potential Conflicts of Interest

No potential conflicts of interest were disclosed.

Grant Support

This work was supported by an UEF talent grant of the Van der Meer-Boerema Foundation and Dutch Cancer Society grants 2010-4739, 2010-4603 and 2007-3739.

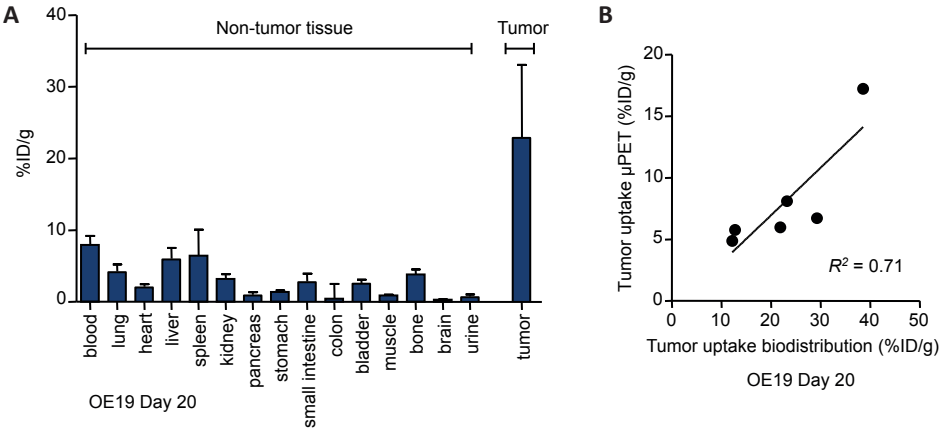

Supplemental Figure 1

(A) Day 20 *ex vivo* biodistribution data of ^{89}Zr-trastuzumab, in mice bearing OE19 treated with bevacizumab (5 mg/kg) on day 13, 16 and 19. The %ID/g ± SD is shown for non-tumor tissue and tumor for ^{89}Zr-trastuzumab. (B) The day 20 *ex vivo* biodistribution tumor uptake (%ID/g) in the OE19 model correlated with the day 20 *in vivo* PET tumor uptake (%ID/g), R^2 = 0.71 for OE19.

References

1. Hanahan D, Weinberg RA. Hallmarks of cancer: The next generation. Cell 2011;11:646-74.
2. Ferrara N, Gerber HP, LeCouter J. The biology of VEGF and its receptors. Nat Med 2003;9:669-76.
3. Carmeliet P, Jain RK. Principles and mechanisms of vessel normalization for cancer and other angiogenic diseases. Nat Rev Drug Discov 2011;10:417-27.
4. Goel S, Duda DG, Xu L, Munn LL, Boucher Y, Fukumura D et al. Normalization of the vasculature for treatment of cancer and other diseases. Physiol Rev 2011;91:1071-121.
5. Ozerdem U, Stallcup WB. Early contribution of pericytes to angiogenic sprouting and tube formation. Angiogenesis 2003;6:241-49.
6. Yuan F, Chen Y, Dellian M, Safabakhsh N, Ferrara N, Jain RK. Time-dependent vascular regression and permeability changes in established human tumor xenografts induced by an anti-vascular endothelial growth factor/vascular permeability factor antibody. Proc Natl Acad Sci USA 1996;93:14765-70.
7. Tong RT, Boucher Y, Kozin SV, Winkler F, Hicklin DJ, Jain RK. Vascular normalization by vascular endothelial growth factor receptor 2 blockade induces a pressure gradient across the vasculature and improves drug penetration in tumors. Cancer Res 2004;64:3731-6.
8. Winkler F, Kozin SV, Tong RT, Chae SS, Booth MF, Garkavtsev I et al. Kinetics of vascular normalization by VEGFR2 blockade governs brain tumor response to radiation: role of oxygenation, angiopoietin-1, and matrix metalloproteinases. Cancer Cell. 2004;6:553-63.
9. Jain RK. Normalizing tumor vasculature with anti-angiogenic therapy: a new paradigm for combination therapy. Nat Med 2001;9:987-9.
10. Jain RK. Normalization of tumor vasculature: an emerging concept in antiangiogenic therapy. Science 2005;307:58-62.
11. Dickson PV, Hammer JB, Sims TL, Fraga CH, Ng CY, Rajasekeran S et al. Bevacizumab-induced transient remodeling of the vasculature in neuroblastoma xenografts results in improved delivery and efficacy of systemically administered chemotherapy. Clin Cancer Res 2007;13:3942-50.
12. Wildiers H, Guetens G, De Boeck G, Verbeken E, Landuyt B, Landuyt W et al. Effect of antivascular endothelial growth factor treatment on the intratumoral uptake of CPT-11. Br J Cancer 2003;88:1979-86.
13. Carmeliet P, Jain RK. Principles and mechanisms of vessel normalization for cancer and other angiogenic diseases. Nat Rev Drug Discov 2011;10:417-27.
14. van der Veldt AA, Lubberink M, Bahce I, Walraven M, de Boer MP, Greuter HN et al. Rapid decrease in delivery of chemotherapy to tumors after anti-VEGF therapy: implications for scheduling of anti-angiogenic drugs. Cancer Cell 2012;21:82-91.
15. von Minckwitz G, Eidtmann H, Rezai M, Fasching PA, Tesch H, Eggemann H et al. Neoadjuvant chemotherapy and bevacizumab for HER2-negative breast cancer. N Engl J Med 2012;366:299-309.
16. Bear HD, Tang G, Rastogi P, Geyer CE, Robidoux A, Atkins JN et al. Bevacizumab added to neoadjuvant chemotherapy for breast cancer. N Engl J Med 2012;366:310-20.
17. Maeda H, Wu J, Sawa T, Matsumura Y, Hori, K. Tumor vascular permeability and the EPR effect in macromolecular therapeutics: a review. J Control Release 2000;65:271-84.
18. Nakahara T, Norberg SM, Shalinsky DR, Hu-Lowe DD, McDonald DM. Effect of inhibition of vascular endothelial growth factor signaling on distribution of extravasated antibodies in tumors. Cancer Res. 2006;66:1434-45.

19. Tol J, Koopman M, Cats A, Rodenburg CJ, Creemers GJ, Schrama JG et al. Chemotherapy, bevacizumab, and cetuximab in metastatic colorectal cancer. N Engl J Med 2009;360:563-72.
20. Hecht JR, Mitchell E, Chidiac T, Scroggin C, Hagenstad C, Spigel D et al. A randomized phase IIIB trial of chemotherapy, bevacizumab, and panitumumab compared with chemotherapy and bevacizumab alone for metastatic colorectal cancer. J Clin Oncol 2009;27:672-80.
21. Gianni L, Romieu G, Lichinitser M, Serrano S, Mansutti M, Pivot X et al. First results of AVEREL, a randomized phase III trial to evaluate bevacizumab (BEV) in combination with trastuzumab (H) + docetaxel (DOC) as first-line therapy for HER2-positive locally recurrent/metastatic breast cancer (LR/mBC). SABCS 2011; abstract S4-8.
22. Arteaga CL, Mayer IA, O'Neill AM, Swaby RF, Alpaugh RK, Yang XJ et al. A randomized phase III double-blinded placebo-controlled trial of first-line chemotherapy and trastuzumab with or without bevacizumab for patients with HER2/neu-overexpressing metastatic breast cancer (HER2+ MBC): A trials of the Eastern Cooperative Oncology Group (E1105). J Clin Oncol 2012;30:(suppl; abstr 605).
23. Nagengast WB, de Vries EG, Hospers GA, Mulder NH, de Jong JR, Hollema H et al. In vivo VEGF imaging with radiolabeled bevacizumab in a human ovarian tumor xenograft. J Nucl Med 2007;48:1313-9.
24. Dijkers EC, Oude Munnink TH, Kosterink JG, Brouwers AH, Jager PJ, de Jong J et al. HER2 PET imaging with ^{89}Zr-trastuzumab in metastatic breast cancer patients. Clin Pharmacol Ther 2010; 87:586-92.
25. Dijkers ECF, Kosterink JG, Rademaker AP, Perk LR, Dongen van GA, Bart J et al. Development and characterization of clinical-grade ^{89}Zr-trastuzumab for HER2/neu immunoPET imaging. J Nucl Med 2009; 50:962-9.
26. Terwisscha van Scheltinga AG, van Dam GM, Nagengast WB, Ntziachristos V, Hollema H, Herek JL et al. Intraoperative near-infrared fluorescence tumor imaging with vascular endothelial growth factor and human epidermal growth factor receptor 2 targeting antibodies. J Nucl Med 2011;52:1778-85.
27. Keyes KA, Mann L, Teicher B, Alvarez E. Site-dependent angiogenic cytokine production in human tumor xenografts. Cytokine 2003;21:98-104.
28. Dahlberg PS, Jacobson BA, Dahal G, Fink JM, Kratzke RA, Maddaus MA, Ferrin LJ. ERBB2 amplifications in esophageal adenocarcinoma. Ann Thorac Surg 2004;78:1790-800.
29. Reddy N, Ong GL, Behr TM, Sharkey RM, Goldenberg DM, Mattes MJ. Rapid blood clearance of mouse IgG2a and human IgG1 in many nude and nu/+ mouse strains is due to low IgG2a serum concentrations. Cancer Immunol Immunother 1998;46:25-33.
30. Gerber HP, Ferrara N. Pharmacology and pharmacodynamics of bevacizumab as monotherapy or in combination with cytotoxic therapy in preclinical studies. Cancer Res 2005;65:671-80.
31. Oude Munnink TH, de Vries EG, Vedelaar SR, Timmer-Bosscha H, Schröder CP, Brouwers AH et al. Lapatinib and 17AAG reduce ^{89}Zr-trastuzumab-F(ab')2 uptake in SKBR3 tumor xenografts. Mol Pharm. 2012;9:2995-3002.
32. Willett CG, Duda DG, di Tomaso E, Boucher Y, Ancukiewicz M, Sahani DV, et al. Efficacy, safety, and biomarkers of neoadjuvant bevacizumab, radiation therapy, and fluorouracil in rectal cancer: a multidisciplinary phase II study. J Clin Oncol 2009;27:3020-6.
33. Batchelor TT, Sorensen AG, di Tomaso E, Zhang WT, Duda DG, Cohen KS, et al. AZD2171, a pan-VEGF receptor tyrosine kinase inhibitor, normalizes tumor vasculature and alleviates edema in glioblastoma patients. Cancer Cell 2007;11:83-95.

34. Chauhan VP, Stylianopoulos T, Martin JD, Popovíc Z, Chen O, Kamoun WS et al. Normalization of tumor blood vessels improves the delivery of nanomedicines in a size-dependent manner. Nat Nanotechnol 2012; 7:383-8.

35. Pastuskovas CV, Mundo EE, Williams SP, Nayak TK, Ho J, Ulufatu S et al. Effects of anti-VEGF on pharmacokinetics, biodistribution and tumor penetration of trastuzumab in a preclinical breast cancer model. Mol Cancer Ther 2012;11:752-62.

36. Le XF, Mao W, Lu C, Thornton A, Heymach JV, Sood AK et al. Specific blockade of VEGF and HER2 pathways results in greater growth inhibition of breast cancer xenografts that overexpress HER2. Cell Cycle. 2008;7:3747-58.

37. Traina TA, Higgins B, Theodoulou M, Dugan U, Kolinsky K,Zhang Y et al. Preclinical testing of a novel regimen of capecitabine (C) in combination with bevacizumab (B) and trastuzumab (T) in a breast cancer xenograft model. J Clin Oncol 2007;25:(suppl; abstr 1049).

38. Clynes RA, Towers TL, Presta LG, Ravetch JV. Inhibitory Fc receptors modulate in vivo cytotoxicity against tumor targets. Nat Med 2000;6:443-6.

39. zum Büschenfelde CM, Hermann C, Schmidt B, Peschel C, Bernhard H. Antihuman epidermal growth factor receptor 2 (HER2) monoclonal antibody trastuzumab enhances cytolytic activity of class I-restricted HER2-specific T lymphocytes against HER2-overexpressing tumor cells. Cancer Res 2002;62:2244-7.

40. Wolpoe ME, Lutz ER, Ercolini AM, Murata S, Ivie SE, Garrett ES et al. HER-2/neu-specific monoclonal antibodies collaborate with HER-2/neu-targeted granulocyte macrophage colony-stimulating factor secreting whole cell vaccination to augment CD8+ T cell effector function and tumor-free survival in Her-2/neu-transgenic mice. J Immunol 2003;171:2161-9.

41. Gennari R, Menard S, Fagnoni F, Ponchio L, Scelsi M, Tagliabue E et al. Pilot study of the mechanism of action of preoperative trastuzumab in patients with primary operable breast tumors overexpressing HER2. Clin Cancer Res 2004;10:5650-5.

42. Jonker DJ, O'Callaghan CJ, Karapetis CS, Zalcberg JR, Tu D, Au HJ et al. Cetuximab for the treatment of colorectal cancer. N Engl J Med 2007;357:2040-8.

43. Cunningham D, Humblet Y, Siena S, Khayat D, Bleiberg H, Santoro A et al. Cetuximab monotherapy and cetuximab plus irinotecan in irinotecan refractory metastatic colorectal cancer. N Engl J Med 2004;351:337-35.

44. Pander J, Heusinkveld M, van der Straaten T, Jordanova ES, Baak-Pablo R, Gelderblom H et al. Activation of tumor-promoting type 2 macrophages by EGFR-targeting antibody cetuximab. Clin Cancer Res 2011; 17:5668-73.

45. Oosting SF, Brouwers AH, Van Es SC, Nagengast WB, Oude Munnink TH, Lub-de Hooge MN et al. ^{89}Zr-bevacizumab PET imaging in metastatic renal cell carcinoma patients before and during antiangiogenic treatment. J Clin Oncol 2012;30:(suppl; abstr 10581).